

# Dissociation of Alkaliated Alanine in the Gas Phase: The Role of the Metal Cation

Seduraman Abirami,<sup>[a, b]</sup> Catherine Chiu Lan Wong,<sup>[c]</sup> Chun Wai Tsang,<sup>\*, [d]</sup> and Ngai Ling Ma<sup>\*, [b]</sup>

**Abstract:** The dissociation of prototypical metal-cationized amino acid complexes, namely, alkaliated alanine ( $[\text{Ala}+\text{M}]^+$ ,  $\text{M}^+ = \text{Li}^+, \text{Na}^+, \text{K}^+$ ), was studied by energy-resolved tandem mass spectrometry with an ion-trap mass analyzer and by density functional theory. Dissociation leads to formation of fragment ions arising from the loss of small neutrals, such as  $\text{H}_2\text{O}$ ,  $\text{CO}$ ,  $\text{NH}_3$ ,  $(\text{CO}+\text{NH}_3)$ , and the formation of  $\text{Na}^+/\text{K}^+$ . The order of appearance threshold voltages for different dissociation pathways determined experimentally is consistent with the order of critical energies (energy barriers) obtained

theoretically, and this provides the necessary confidence in both experimental and theoretical results. Although not explicitly involved in the reaction, the alkali metal cation plays novel and important roles in the dissociation of alkaliated alanine. The metal cation not only catalyzes the dissociation (via the formation of loosely bound ion–molecule complexes and by stabilizing the


**Keywords:** alkali metals • amino acids • density functional calculations • ion fragmentation • mass spectrometry

more polar intermediates and transition structures), but also affects the dissociation mechanisms, as the cation can alter the shape of the potential energy surfaces. This compression/expansion of the potential energy surface as a function of the alkali metal cation is discussed in detail, and how this affects the competitive loss of  $\text{H}_2\text{O}$  versus  $\text{CO}/(\text{CO}+\text{NH}_3)$  from  $[\text{Ala}+\text{M}]^+$  is illustrated. The present study provides new insights into the origin of the competition between various dissociation channels of alkaliated amino acid complexes.

## Introduction

The rapid development of proteomics has placed a high demand on the use of tandem mass spectrometry (MS/MS) to determine the sequence of peptides generated by specific proteolytic enzymes.<sup>[1]</sup> At present, peptide sequencing by mass spectrometry is routinely carried out by interpreting the low-energy (eV scale, laboratory frame) collision-induced dissociation (CID) mass spectra of protonated ( $\text{H}^+$ ) peptides, which generally reveal extensive fragmentation due to the “mobility” of the added proton.<sup>[2]</sup>  $\text{Na}^+$  and  $\text{K}^+$  ions are ubiquitous in biological systems, and their adduct ions with peptides are commonly observed in the mass spectra of biological samples. The CID of alkaliated ( $\text{M}^+ = \text{Li}^+, \text{Na}^+, \text{K}^+$ ) peptides in the gas phase has been investigated by several research groups, and found to yield sequence information complementary to that obtained from protonated peptides.<sup>[3–8]</sup> Despite the complementary use of CID-MS/MS spectra of alkaliated peptides for sequence determination, the mechanistic details of the dissociation processes remain largely unknown. A better understanding of the dissociation pathways and mechanisms, especially the role played by the

- [a] S. Abirami  
National Institute of Education, Science and Technology Education  
1 Nanyang Walk, 637616 (Singapore)
- [b] S. Abirami, Dr. N. L. Ma  
Institute of High Performance Computing  
1 Science Park Road, No. 01-01, The Capricorn  
Singapore Science Park II, 117528 (Singapore)  
Fax: (+65) 677-80-522  
E-mail: ida@ihpc.a-star.edu.sg
- [c] C. C. L. Wong  
Department of Chemistry  
The University of Hong Kong  
Pokfulam Road (Hong Kong)
- [d] Prof. C. W. Tsang  
Department of Applied Biology and Chemical Technology and  
Institute of Molecular Technology for Drug Discovery and Synthesis  
An Area of Excellence of the University Grants Committee (Hong Kong)  
The Hong Kong Polytechnic University, Hung Hom (Hong Kong)  
Fax: (+852) 236-49-932  
E-mail: bcctsang@polyu.edu.hk

 Supporting information for this article is available on the WWW under <http://www.chemurj.org/> or from the authors.

alkali metal cation, is not only of fundamental interest, but also has practical relevance to the future development of alternative MS/MS techniques for peptide sequencing.

The simplest fragmentation models of peptides/proteins are those of protonated/alkaliated amino acids, as the fragment ions derived from the dissociation of amino acids are often found in the CID-MS/MS spectra of small peptides. In CID of protonated amino acids, which has been studied extensively, loss of stable small neutral molecules, such as H<sub>2</sub>O, NH<sub>3</sub>, CO, and combination or consecutive loss of these species, are common, and dissociation is believed to be initiated by proton shifts.<sup>[9]</sup> In the present study, the loss of small neutral molecules such as H<sub>2</sub>O, NH<sub>3</sub>, and (CO+NH<sub>3</sub>), are also found to be the major dissociation pathways of alkaliated amino acids. However, in comparison with the corresponding protonated systems the alkaliated forms are proton-deficient, so the dissociation mechanisms are very likely to be different from those of the protonated analogues.

Theoretical studies on the dissociation mechanisms of metal-cationized amino acids have been reported in the literature, but these studies focused on transition-metal cations such as Ni<sup>+</sup>,<sup>[10]</sup> Cu<sup>+</sup>,<sup>[11]</sup> Ag<sup>+</sup>,<sup>[12]</sup> and Zn<sup>2+</sup>.<sup>[13]</sup> Because of the strong cation–ligand interaction, transition-metal cations often initiate dissociation by inserting into various covalent bonds present in the ligand.<sup>[14]</sup> Such a “bond-insertion” mechanism is not likely to be found in the case of alkaliated amino acids, as the largely electrostatic alkali metal cation–ligand interaction is too weak to overcome the energy penalty of breaking the covalent bonds in the ligand.

The dissociation of alkaliated amino acids has not attracted much attention. Even though many studies on stable M<sup>+</sup> binding modes have been reported,<sup>[15]</sup> there are only a very limited number of studies on the rearrangement/interconversion between these M<sup>+</sup> binding modes.<sup>[16]</sup> These studies found that different modes of M<sup>+</sup> binding show the same order of relative binding affinities, that is, Li<sup>+</sup> > Na<sup>+</sup> > K<sup>+</sup>, with little cation selectivity observed.<sup>[15e,f,h,i,n,16]</sup> Recent combined experiment and theoretical studies on Li<sup>+</sup>–glycylglycine also suggest that Li<sup>+</sup> does not have a direct role in the dissociation of the dipeptide.<sup>[8]</sup> However, more in-depth studies are desired to ascertain the roles played by different alkali metal cations in the CID of alkaliated amino acids/peptides.<sup>[17]</sup>

In this work, we have carried out a combined experimental and DFT study on the dissociation of a prototypical alkaliated aliphatic amino acid, namely, alkaliated alanine [Ala+M]<sup>+</sup> (M<sup>+</sup> = Li<sup>+</sup>, Na<sup>+</sup>, K<sup>+</sup>). The CID of [Ala+M]<sup>+</sup> was investigated by energy-resolved tandem mass spectrometry with an ion-trap mass analyzer, that is, recording the appearance and % relative abundances of fragment ions as a function of collision energy (eV scale, laboratory frame) between the [Ala+M]<sup>+</sup> precursor ions and the helium buffer gas in the ion-trap mass analyzer. We found that the order of appearance threshold voltages for fragment ions is qualitatively consistent with the order of theoretical critical energies of dissociation on the potential energy surface, and

this lends support to the validity of both the experimental and theoretical results. We will show experimentally that, contrary to what might have been expected, the fragment ions arising from the dissociation of [Ala+M]<sup>+</sup> complexes are dependent on the nature of M<sup>+</sup>. Based on the theoretical findings, the role of the alkali cation in the gas phase dissociation of alkaliated alanine is elucidated.

## Results and Discussion

### Dissociation of [Ala+Li]<sup>+</sup>

**CID-MS/MS spectra:** The low-energy CID-MS/MS mass spectrum of lithiated alanine [Ala+Li]<sup>+</sup> (*m/z* 96), is shown in Figure 1a. As in the case of protonated alanine,<sup>[9]</sup> loss of CO is also dominant in lithiated alanine, leading to the formation of [Ala+Li–CO]<sup>+</sup> (*m/z* 68). Other significant fragment ions, [Ala+Li–NH<sub>3</sub>]<sup>+</sup> (*m/z* 79), [Ala+Li–H<sub>2</sub>O]<sup>+</sup> (*m/z* 78) and [Ala+Li–(CO+NH<sub>3</sub>)]<sup>+</sup> (*m/z* 51), not found in the dissociation of protonated alanine, were also observed. The CID-MS/MS spectra (not shown) of ESI-generated lithiated [D<sub>3</sub>]alanine (ND<sub>2</sub>CH(CH<sub>3</sub>)COOD) and ([D<sub>3</sub>]methyl)alanine (NH<sub>2</sub>CH(CD<sub>3</sub>)COOH) not only confirmed the loss of H<sub>2</sub>O and NH<sub>3</sub> as neutral molecules, they also indicated that H/D of the amino (NH<sub>2</sub>/ND<sub>2</sub>) and carboxyl group (COOH/COOD) are involved in these reactions.

The experimental breakdown graph for the dissociation of [Ala+Li]<sup>+</sup>, which consists of plots of percentage fragment/total ion abundance versus RF activation voltage (collision energy) applied to the end-cap electrodes of the ion trap mass analyzer, is shown in Figure 2a. For [Ala+Li]<sup>+</sup>, plots of percentage fragment ion intensity (the intensity of the precursor ion [Ala+Li]<sup>+</sup> is excluded from the calculation of percentage ion intensities) instead of percentage total ion intensity (the intensity of the precursor ion is included in the calculation of percentage ion intensities) is used to amplify graphically the variation of fragment ion intensities in the threshold voltage region. From these plots (curves), the order of threshold RF voltages (in V) for observing the appearance of the various fragment ions (–neutral with threshold voltages [V] in parentheses) can be estimated: [Ala+Li]<sup>+</sup>: –CO (0.25) < –H<sub>2</sub>O (0.29) ≈ –(CO+NH<sub>3</sub>) (0.29) < –NH<sub>3</sub> (0.41).

This order of threshold voltages was found to be reproducible and remain unchanged as the *q<sub>z</sub>* value of the ion trap was varied from 0.2 to 0.3. The breakdown curves clearly show that the loss of CO is the energetically preferred dissociation pathway of [Ala+Li]<sup>+</sup>, while the pathway leading to the loss of NH<sub>3</sub> is likely to have the highest energy barrier.

**Overview of the potential energy surface:** In the discussion below, the notation **1**, **2**, etc., is used to denote the corresponding species of alkaliated alanine [Ala+Li/Na/K]<sup>+</sup> collectively, while **1Li**, **1Na**, and **1K**, and so on, are reserved for the species **1** of lithiated, sodiated, or potassiated alanine, respectively.

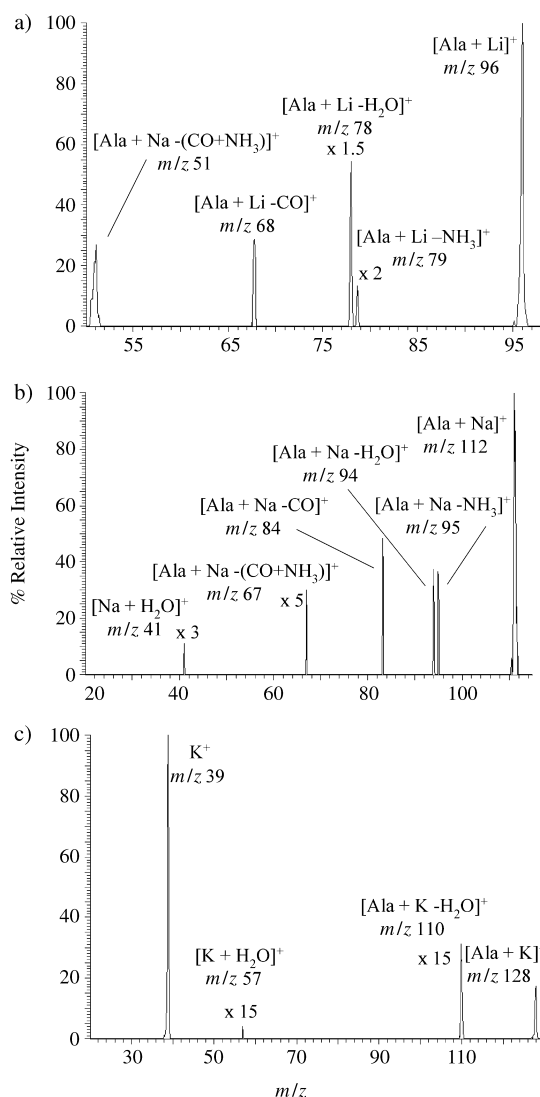


Figure 1. Low-energy ion-trap CID mass spectra of a) lithiated alanine  $[\text{Ala}+\text{Li}]^+$  ( $m/z$  96), RF activation voltage 0.45 V; b) sodiated alanine  $[\text{Ala}+\text{Na}]^+$  ( $m/z$  112), RF activation voltage 0.44 V; and c) potassiated alanine  $[\text{Ala}+\text{K}]^+$  ( $m/z$  128), RF activation voltage 0.58 V. (Ion-trap conditions: low-mass scan mode with the main RF voltage of the ring electrode adjusted and optimized as described in Experimental Details, ion-activation time 5 ms, trap offset of  $-5$  V and  $q_z$  of 0.2).

The potential energy surface for the loss of  $\text{H}_2\text{O}$ ,  $\text{CO}$ ,  $\text{NH}_3$ , and  $(\text{CO}+\text{NH}_3)$  from lithiated alanine, calculated at the B3LYP/6-311+G(3df,2p)//B3-LYP/6-31G(d) level, is shown in Figure 3. The optimized structures of the various species involved in the dissociation of  $[\text{Ala}+\text{M}]^+$  ( $\text{M}^+=\text{Li}^+$ ,  $\text{Na}^+$ ,  $\text{K}^+$ ) are summarized in Figure 4. The relative enthalpies at 0 K ( $\Delta H_0$  relative to species **1**) are summarized in Table 1, and the relative enthalpies and Gibbs free energies at 298 K can be found in Supporting Information, Table S1.

As summarized in Table 2, the order of theoretical critical energy for the loss of  $\text{H}_2\text{O}$ ,  $\text{CO}$ , and  $\text{NH}_3$  pathways (in  $\text{kJ mol}^{-1}$ ) is:  $[\text{Ala}+\text{Li}]^+$ :  $-\text{CO}$  (177)  $\approx$   $-(\text{CO}+\text{NH}_3)$  (177)  $<$   $-\text{H}_2\text{O}$  (182)  $<$   $-\text{NH}_3$  (206).

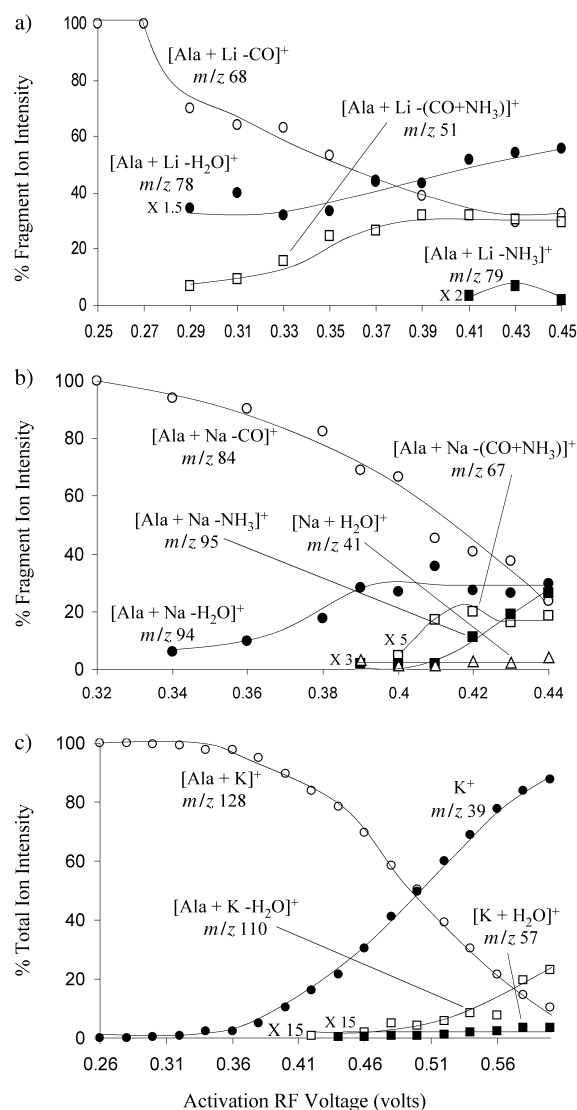


Figure 2. Ion-trap energy-resolved MS/MS breakdown graph of a) lithiated alanine  $[\text{Ala}+\text{Li}]^+$  ( $m/z$  96), b) sodiated alanine  $[\text{Ala}+\text{Na}]^+$  ( $m/z$  112), and c) potassiated alanine  $[\text{Ala}+\text{K}]^+$  ( $m/z$  128). Ion-trap conditions were the same as in Figure 1.

This order is in qualitative agreement with the order of observed ion-trap threshold voltages, as shown in the previous section. In this regard, we note that the multistep collisional excitation conditions and extended time window (tens of milliseconds) of an ion-trap mass analyzer have been shown to favor the observation of dissociation pathways with low critical energies.<sup>[18]</sup> Furthermore, kinetic shift effects, which shift the experimental threshold voltages to higher values, are much smaller in the ion trap than in other types of tandem mass spectrometer (e.g., B-E sector or triple quadrupole) operated in the microsecond time frame.<sup>[19]</sup> Mainly for these reasons, previous studies have shown that the critical energies for dissociation of small molecular ions (with  $m/z$  values in the same range as  $[\text{Ala}+\text{M}]^+$  in this study) can be correlated to the experimental collision energies, that is, the appearance threshold

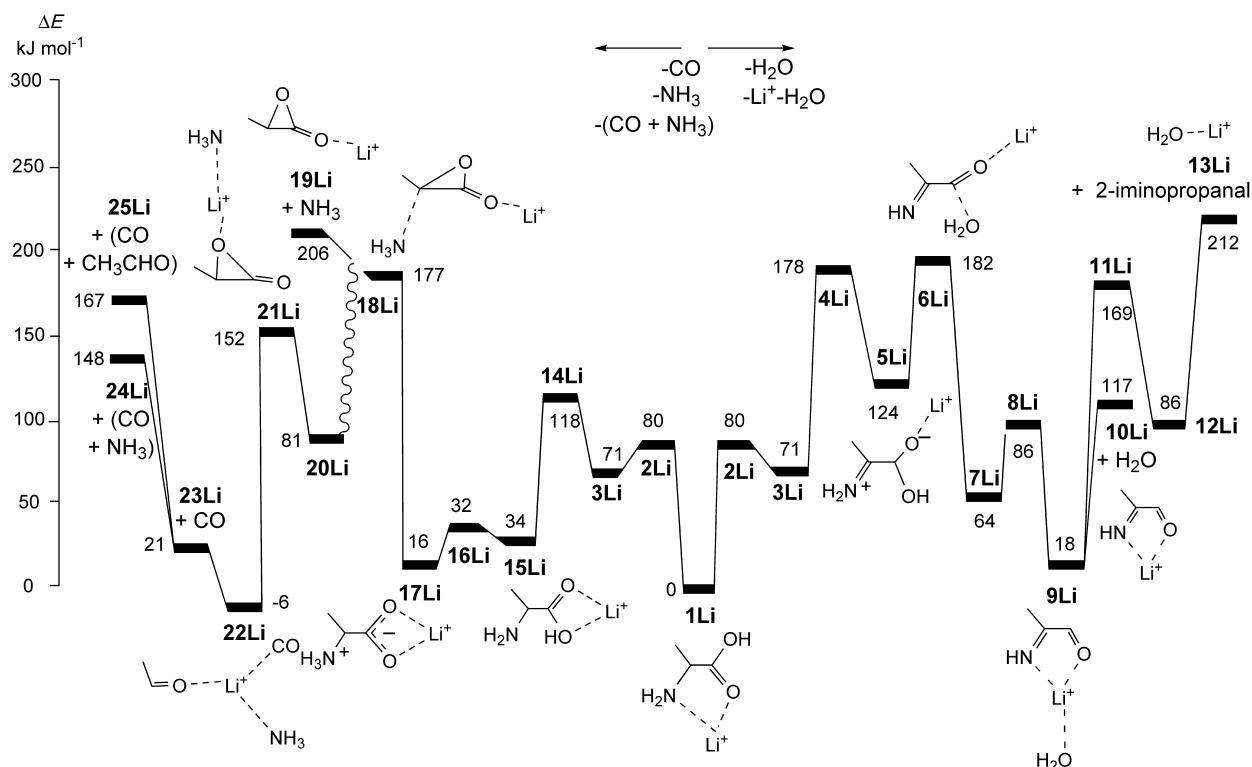


Figure 3. Potential energy surface of the dissociation of  $[\text{Ala}+\text{Li}]^+$  leading to the loss of  $\text{H}_2\text{O}$ ,  $\text{NH}_3$ ,  $\text{CO}$ , and  $(\text{CO}+\text{NH}_3)$ : all species are stable intermediates/products, except **2Li**, **4Li**, **6Li**, **8Li**, **11Li**, **14Li**, **16Li**, and **21Li**, which are transition structures.

Table 1. The  $[\text{Ala}+\text{M}]^+$  ( $\text{M}^+=\text{Li}^+$ ,  $\text{Na}^+$  and  $\text{K}^+$ ) potential energy surface: relative enthalpies at 0 K ( $\Delta H_0$  [ $\text{kJ mol}^{-1}$ ]).<sup>[a]</sup>

Species	$\text{Li}^+$	$\text{Na}^+$	$\text{K}^+$
<b>2</b>	80	60	39
<b>3</b>	71	51	30
<b>4</b>	178	174	162
<b>5</b>	124	131	124
<b>6</b>	182	176	165
<b>7</b>	64	69	70
<b>8</b>	86	90	91
<b>9</b>	18	35	52
<b>10</b> + $\text{H}_2\text{O}$	117	108	102
<b>11</b>	169	181	183
<b>12</b>	86	89	89
<b>13</b> +2-iminopropanal	212	179	151
<b>14</b>	118	95	74
<b>15</b>	34	10	−6
<b>16</b>	32	11	0
<b>17</b>	16	6	1
<b>18</b>	177	155	136
<b>19</b> + $\text{NH}_3$	206	181	158
<b>20</b>	81	90	99
<b>21</b>	152	170	183
<b>22</b>	−6	9	25
<b>23</b> + $\text{CO}$	21	31	39
<b>24</b> + $(\text{CO}+\text{NH}_3)$	148	123	99
<b>25</b> + $(\text{CO}+\text{CH}_3\text{CHO})$	167	139	119

[a] Relative to **1** (Figures 3 and 4). [b] The electronic energies (corrected by zero-point vibration energy) for **1Li**, **1Na**, and **1K** are  $-331.15073$ ,  $-485.92425$ , and  $-923.57586$  Hartree, respectively.

(onset) radio-frequency (RF) activation voltages for observation of the corresponding fragment ions in an ion-trap mass analyzer.<sup>[20,21]</sup> We stress that the qualitative correlation between the order of theoretical critical energies and ion-trap threshold voltages reported here is limited to fragment ions derived from the same precursor ion (i.e., within col-

Table 2. Theoretical critical energy [ $\text{kJ mol}^{-1}$ ] for the formation of  $\text{M}^+$  and loss of small neutrals on the  $[\text{Ala}+\text{M}]^+$  ( $\text{M}^+=\text{Li}^+$ ,  $\text{Na}^+$ ,  $\text{K}^+$ ) potential energy surface.<sup>[a]</sup>

$\text{M}^+$ formation/neutral loss	$[\text{Ala}+\text{Li}]^+$	$[\text{Ala}+\text{Na}]^+$	$[\text{Ala}+\text{K}]^+$
$\text{M}^+$ <sup>[b]</sup>	251 (− <sup>[c]</sup> )	174 (0.34 <sup>[d]</sup> )	123 (0.26)
$\text{CO}$ <sup>[e]</sup>	177 (0.25)	170 (0.32)	183 (− <sup>[c]</sup> )
$\text{H}_2\text{O}$ <sup>[f]</sup>	182 (0.29)	176 (0.34)	165 (0.42)
$\text{NH}_3$ <sup>[g]</sup>	206 (0.41)	181 (0.39)	158 (− <sup>[c]</sup> )
$(\text{CO}+\text{NH}_3)$ <sup>[e]</sup>	177 (0.29)	170 (0.40)	183 (− <sup>[c]</sup> )
$[\text{M}+\text{H}_2\text{O}]^+$ <sup>[h]</sup>	212 (− <sup>[c]</sup> )	181 (0.39)	183 (0.44)

[a] The appearance threshold energy [V] for these fragments ions under ion-trap CID conditions is shown in parentheses. [b] This work; the theoretical binding affinity of alanine calculated at the B3LYP/6-311+G-(3df,2p)//B3LYP/6-31G(d) level for  $\text{Li}^+$ ,  $\text{Na}^+$ , and  $\text{K}^+$ , respectively. [c] Not observed under ion-trap CID conditions. [d] Appearance threshold voltage monitored with the main RF amplitude (voltage) of the ring electrode optimized at  $m/z$  23 (see Experimental Details and text). [e] For  $\text{Li}^+$ : via intermediate species **18Li**; for  $\text{Na}^+$  and  $\text{K}^+$ : via transition structures **21Na** and **21K**, respectively (Figures 3 and 4). [f] Via transition structure **6** (Figures 3 and 4). [g] Formation of intermediate species **19** (Figures 3 and 4). [h] For  $\text{Li}^+$ : formation of product species **13Li**+2-iminopropanal; for  $\text{Na}^+$  and  $\text{K}^+$ : via transition structures **11Na** and **11K**, respectively (Figure 3 and Figure 4).

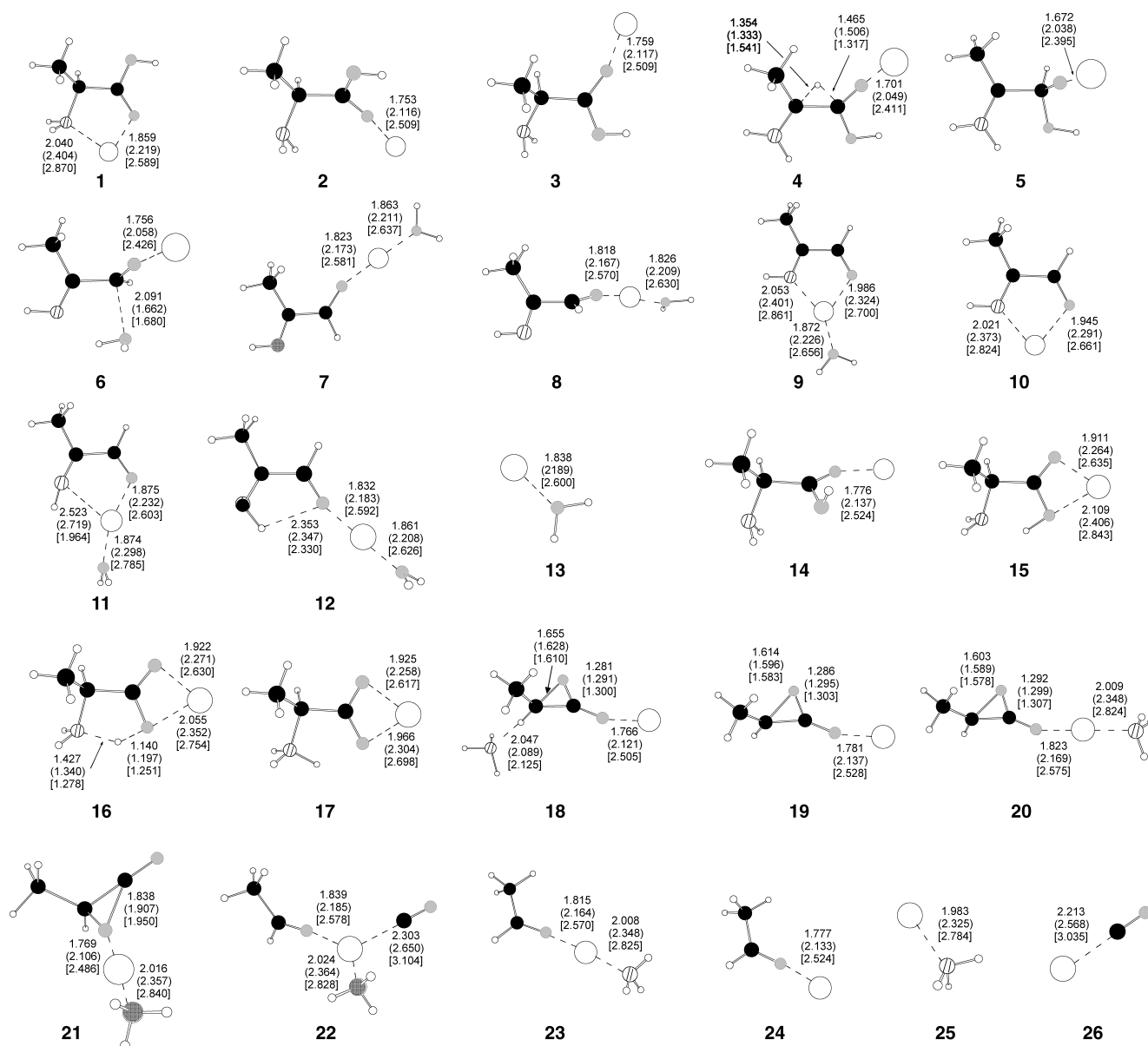


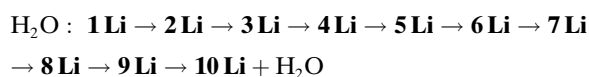
Figure 4. Optimized structures for the various species on the  $[\text{Ala}+\text{M}]^+$  ( $\text{M}^+=\text{Li}^+, \text{Na}^+, \text{K}^+$ ) dissociation potential energy surface: all species are stable intermediates/products, except **2Li**, **4Li**, **6Li**, **8Li**, **11Li**, **14Li**, **16Li**, and **21Li**, which are transition structures. The parameters associated with  $\text{Na}^+$  and  $\text{K}^+$  are given in parentheses and brackets, respectively.

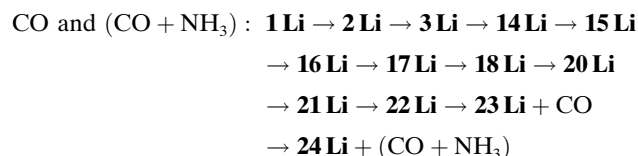
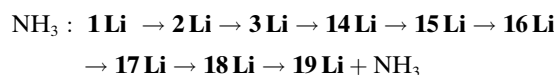
umns of Table 2), but not between different alkylated systems (i.e., across a row of Table 2).

We noted that the pathways for loss of CO and  $(\text{CO}+\text{NH}_3)$  share the same barrier (via intermediate species **18Li**, with critical energy of  $177 \text{ kJ mol}^{-1}$ , Figure 3), yet the two pathways show slightly different threshold voltages:  $-\text{CO}$  ( $0.25 \text{ V}$ )  $<$   $-(\text{CO}+\text{NH}_3)$  ( $0.29 \text{ V}$ ). As shown in the breakdown curves of Figure 2a, in the threshold region, the percentage fragment ion abundance of  $[\text{Ala}+\text{Li}-(\text{CO}+\text{NH}_3)]^+$  increases rapidly at the expense of corresponding decrease in  $[\text{Ala}+\text{Li}-\text{CO}]^+$  fragment-ion abundance. This indicates that the  $[\text{Ala}+\text{Li}-(\text{CO}+\text{NH}_3)]^+$  fragment ion is very likely to be formed from sequential loss of CO and  $\text{NH}_3$  (loss of CO prior to loss of  $\text{NH}_3$ ), so that a slightly higher collisional

energy than for loss of CO is needed to drive the further loss of  $\text{NH}_3$  to be detectable by the mass analyzer. In other words, a kinetic-shift effect is probably at work here<sup>[19]</sup> that causes the appearance of  $[\text{Ala}+\text{Li}-(\text{CO}+\text{NH}_3)]^+$  to occur at a slightly higher threshold voltage (ca.  $0.04 \text{ V}$ ) than that of  $[\text{Ala}+\text{Li}-\text{CO}]^+$ . Thus, the theoretical potential energy surface (Figure 3) can be regarded as qualitatively consistent with the experimental observations.

As shown in Figure 3, there are three major dissociation pathways of  $[\text{Ala}+\text{Li}]^+$  from **1Li**, leading to the loss of:

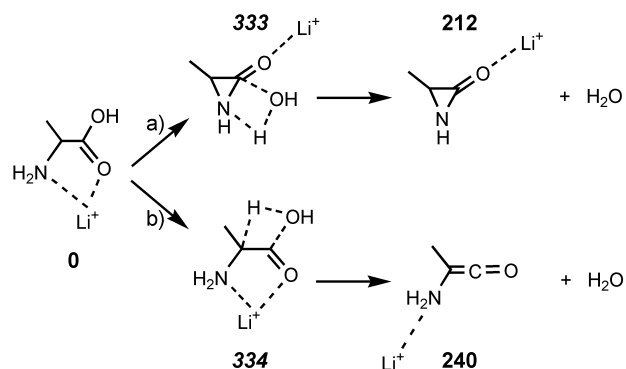




We first present our proposed pathway for the loss of H<sub>2</sub>O from [Ala+Li]<sup>+</sup> (Figure 3).

**Loss of H<sub>2</sub>O:** It is agreed in the literature<sup>[15e,f,16a]</sup> that the most stable mode of Li<sup>+</sup> binding to the Ala ligand is bidentate, with the cation binding to the carbonyl oxygen and amino nitrogen atoms (in *cis* conformation, **1Li**). From this species, via the transition structure **2Li**, a less stable conformer **3Li** (carbonyl group *trans* to the amino group) is formed. With a 1,2-hydrogen shift from C<sup>α</sup> (via transition structure **4Li**), dipolar species **5Li** is formed, in which the N-terminal NH<sub>2</sub> and C-terminal COOH groups are estimated to carry 0.25 and −0.95 a.u. of charge, respectively. A 1,4-hydrogen shift from the amino nitrogen to the hydroxyl oxygen atom follows, via a late transition structure **6Li**, which leads to formation of ion–molecule complex **7Li**. By rotation about the C–C bond (via transition structure **8Li**), a fairly stable ion–molecule complex, **9Li**, in which Li<sup>+</sup> is bound bidentately by 2-iminopropanal (NH=(CH<sub>3</sub>)CHCHO) and monodentately by water, can be formed. This species can dissociate further to yield either H<sub>2</sub>O+**10Li** (lithiated 2-iminopropanal), or via transition structure **11Li** and intermediate **12Li** to yield 2-iminopropanal+**13Li** (lithiated water). In the case of [Ala+Li]<sup>+</sup>, our calculation suggests that H<sub>2</sub>O+**10Li** is about 100 kJ mol<sup>−1</sup> more stable than 2-iminopropanal+**13Li**. Most importantly, 2-iminopropanal+**13Li** (lithiated water) is higher in energy than the barrier associated with the transition structure **6Li**, which suggests that the pathway involving formation of lithiated water is not competitive with that involving formation of lithiated 2-iminopropanal (**10Li**)+H<sub>2</sub>O. This is in line with our experimental observation that the lithiated-water fragment ion [Li+H<sub>2</sub>O]<sup>+</sup> (*m/z* 25), was not found in the CID-MS/MS spectrum of [Ala+Li]<sup>+</sup>.

Previously, loss of H<sub>2</sub>O was also observed in other metal-cationized amino acids ([Gly+Ni]<sup>+</sup><sup>[10]</sup> and [Phe+Ag]<sup>+</sup><sup>[12b,c]</sup>) and was proposed to be associated with the formation of a Ag<sup>+</sup>/Ni<sup>+</sup>-bound α-lactam (aziridinone). Apart from this, the loss of water, along with a Cu<sup>+</sup>-bound α-lactam or aminoketene (NH<sub>2</sub>(CH<sub>3</sub>)CH=C=O) was also considered in the case of [Gly+Cu]<sup>+</sup><sup>[11b]</sup>. We found that, in the case of [Ala+Li]<sup>+</sup>, the energy barriers for the α-lactam and aminoketene pathways are 333 and 334 kJ mol<sup>−1</sup>, respectively (Scheme 1). Both species are clearly higher in energy (by ca. 151 kJ mol<sup>−1</sup>) than the transition structure **6Li**, which leads to the formation of 2-iminopropanal+**13Li** (lithiated water). Thus, for lithiated alanine (and sodiated and potassiumated alanine as well), loss of water should be associated with



Scheme 1. Formation of a) lithiated α-lactam and b) lithiated aminoketene from lithiated alanine (not all species on the dissociation pathways are shown: relative energy [kJ mol<sup>−1</sup>] at 0 K of the minimum in bold, and highest barrier in bold-italic).

the formation of a lithiated 2-iminopropanal (**10Li**). On the other hand, recent studies have suggested that loss of water leading to formation of a metal-bound α-lactam is energetically competitive in the case of Ni<sup>+</sup>,<sup>[10]</sup> but not in the case of Cu<sup>+</sup>.<sup>[11b]</sup> Thus, it appears that the preferred product formed along with the loss of water in metal-cationized amino acids may be dependent on the nature of the metal cation.

**Loss of NH<sub>3</sub>:** As mentioned briefly above, the pathways for the loss of CO, NH<sub>3</sub>, and (CO+NH<sub>3</sub>) from [Ala+Li]<sup>+</sup> are related. From **1Li**, with minor conformation changes (via **2Li**, **3Li**, **14Li**, and **15Li**), a 1,4-hydrogen shift occurs via transition structure **16Li**. The N...H distance is fairly long (1.427 Å, with an estimated bond order of 0.29), while the O...H distance remains rather short (1.140 Å, with a bond order of 0.41), and this implies that **16Li** is an early transition structure. The transition structure **16Li** leads to zwitterionic (ZW) species **17Li**. Loss of NH<sub>3</sub> could occur from **17Li**, via fission of the C<sup>α</sup>–N bond, first forming stable ion–molecule complex **18Li** before yielding lithiated 3-methyloxiran-2-one ion (**19Li**).

**Loss of CO:** Alternatively, the ion–molecule complex **18Li** may rearrange to a more stable ion–molecule complex **20Li**. All our attempts to locate a transition structure linking these two complexes failed. Failing that, we have obtained the variation of potential energy along a plausible reaction coordinate by constrained optimization. Again, no energy maxima could be found. All these findings indicate that the energy barrier to this rearrangement pathway is low, and thus the transition structure is not likely to be important.

Even though we have not been able to locate the transition structure connecting the two complexes, we believe that the rearrangement is highly plausible under the CID excitation conditions of a mass spectrometer. The ion–molecule complex **18Li** can be considered as a lithiated 3-methyloxiran-2-one ion (**19Li**) in which the leaving NH<sub>3</sub> molecule is weakly coordinated to this species by an H–C<sup>α</sup> bond. Given such weak coupling, and if collisional energies are channeled into molecular rotation, the two parts would be tumbling

against each other (as illustrated in Scheme 2), so that the  $\text{NH}_3$  may be “snapped up” by the  $\text{Li}^+$  ion through strong electrostatic interaction.

From **20Li**, via transition structure **21Li**, a weak ion–molecule complex **22Li** is formed, in which the  $\text{Li}^+$  ion is tridentately coordinated to three separate ligands: carbon monoxide (CO), ammonia ( $\text{NH}_3$ ), and acetaldehyde ( $\text{CH}_3\text{CHO}$ ). As the  $\text{Li}^+$ –CO interaction is the weakest of the three  $\text{Li}^+$ –ligand interactions, CO is preferentially lost from **22Li** to form the ion–molecule complex  $[\text{NH}_3\cdots\text{Li}^+\cdots\text{CH}_3\text{CHO}]$  (**23Li**).

**Loss of  $(\text{CO}+\text{NH}_3)$ :** From species **23Li**, further loss of  $\text{NH}_3$  or  $\text{CH}_3\text{CHO}$  may occur to give lithiated acetaldehyde (**24Li**) or lithiated ammonia (**25Li**), respectively. Thermodynamically, the formation of  $[\mathbf{24Li}+\text{CO}+\text{NH}_3]$  is more favorable than  $[\mathbf{25Li}+\text{CO}+\text{CH}_3\text{CHO}]$  by about  $20\text{ kJ mol}^{-1}$  and thus explains the loss of  $(\text{CO}+\text{NH}_3)$  rather than  $(\text{CO}+\text{CH}_3\text{CHO})$  from  $[\text{Ala}+\text{Li}]^+$ . Here we note that our proposed mechanism for the loss of  $(\text{CO}+\text{NH}_3)$  is in line with the observed trends of the breakdown curves, which suggest that loss of CO is followed by  $\text{NH}_3$  (Figure 2a). Since the  $\text{Li}^+$  affinity of  $\text{NH}_3$  is estimated to be larger than that of CO by about  $93\text{ kJ mol}^{-1}$  (at the B3LYP/6-11+G(3df,2p)//B3LYP/6-31G(d) level),<sup>[22]</sup> the alternative mechanism of loss of  $\text{NH}_3$  before CO would be very unlikely. This provides strong indication for the involvement of ion–molecule complexes in the dissociation pathway leading to loss of  $(\text{CO}+\text{NH}_3)$  and indirectly supports the rearrangement of **18Li** to **20Li** as proposed above (Scheme 2).

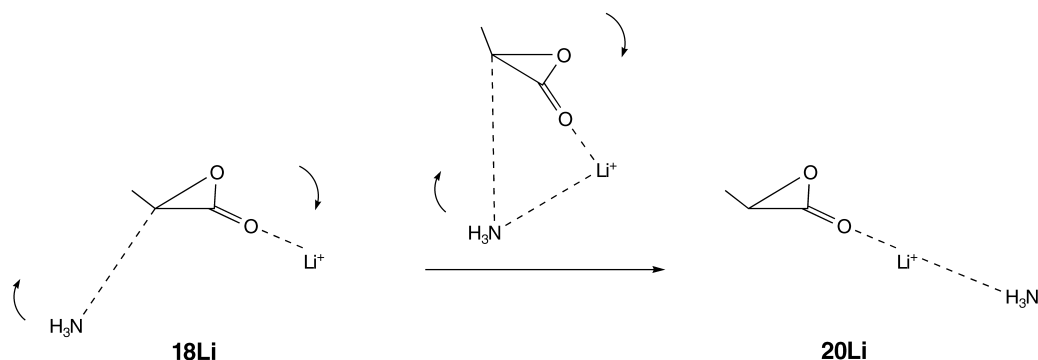
**Dissociation of  $[\text{Ala}+\text{Na}]^+$ :** The low-energy CID-MS/MS mass spectrum of sodiated alanine  $[\text{Ala}+\text{Na}]^+$  ( $m/z$  112) is shown in Figure 1b. Similar to lithiated alanine, fragment ions arising from the loss of CO,  $\text{H}_2\text{O}$ ,  $\text{NH}_3$ , and  $(\text{CO}+\text{NH}_3)$  are observed. In addition, a minor  $[\text{Na}+\text{H}_2\text{O}]^+$  ( $m/z$  41) peak is observed, which presumably is associated with the loss of 2-iminopropanal ( $\text{NH}=\text{CHCHO}$ ) from  $[\text{Ala}+\text{Na}]^+$ . The presence of a corresponding  $[\text{Na}+\text{D}_2\text{O}]^+$  ( $m/z$  43) peak was found in the CID-MS/MS spectrum of ESI-generated sodiated  $[\text{D}_3]\text{alanine}$  ( $\text{ND}_2\text{CH}(\text{CH}_3)\text{COOD}$ ; Figure S1, Supporting Information), suggesting that the

$[\text{Na}+\text{D}_2\text{O}]^+$  ion is formed by direct dissociation of  $[(\text{D}_3)\text{Ala}]+\text{Na}]^+$ .

As shown in Figure 1b, the  $\text{Na}^+$  peak ( $m/z$  23) was not observed under the “normal” ion-trapping conditions described in Experimental Details. This is because the trapping efficiency of the ion-trap mass analyzer becomes highly dependent on  $m/z$  and very poor at such low  $m/z$  values. On reoptimizing (readjusting) the main RF voltage of the ring electrode to  $m/z$  23 (see Figure S2, Supporting Information), the  $\text{Na}^+$  ion was indeed detected. However, under such conditions, the fragment ions with higher  $m/z$  shown in Figure 1b were not efficiently trapped and became undetectable. The direct formation of  $\text{Na}^+$  ion from  $[\text{Ala}+\text{Na}]^+$  was confirmed by separate CID-MS/MS studies with a triple-quadrupole tandem mass spectrometer (Quattro Ultima, Micromass, Manchester, UK).

The experimental breakdown graph for the dissociation of  $[\text{Ala}+\text{Na}]^+$  obtained under “normal” ion-trapping conditions is shown in Figure 2b. We also monitored the appearance threshold voltage of  $\text{Na}^+$  formation when the main RF voltage of the ring electrode was optimized at  $m/z$  23. The appearance threshold voltage (in V) for these dissociation channels is in the order of:  $[\text{Ala}+\text{Na}]^+$ :  $-\text{CO}$  (0.32)  $< \text{Na}^+$  formation (0.34)  $\approx -\text{H}_2\text{O}$  (0.34)  $< -\text{NH}_3$  (0.39)  $\approx [\text{Na}+\text{H}_2\text{O}]^+$  (0.39)  $< -(\text{CO}+\text{NH}_3)$  (0.40).

Good qualitative agreement is observed when these appearance voltages are compared with theoretical critical energies (summarized in Table 2). As in the case of  $[\text{Ala}+\text{Li}]^+$ , the kinetic shift effect in  $[\text{Ala}+\text{Na}]^+$  also leads to the higher threshold voltage observed for loss of  $(\text{CO}+\text{NH}_3)$  versus loss of CO, even though the two pathways share the same barrier. The experimental threshold voltages for  $\text{Na}^+$  formation and loss of  $\text{H}_2\text{O}$  are about the same at 0.34 V, while the theoretical critical energies show a small difference for  $\text{Na}^+$  formation ( $174\text{ kJ mol}^{-1}$ ) and loss of  $\text{H}_2\text{O}$  ( $176\text{ kJ mol}^{-1}$ ). On the one hand, this minor difference can be attributed to the uncertainties in the calculated critical energies. On the other hand, it could also be due to the fact that different main RF trapping voltages were employed to obtain these two threshold voltages.



Scheme 2. Illustration of the relative tumbling of ammonia and lithiated 3-methyloxiran-2-one components in the ion–molecule complex **18Li** leading to formation of the more stable ion–molecule complex **20Li**.

**Dissociation of  $[\text{Ala}+\text{K}]^+$ :** The dissociation characteristics of  $[\text{Ala}+\text{K}]^+$  differ from those of the  $\text{Li}^+$  and  $\text{Na}^+$  analogues. While  $\text{K}^+$  ( $m/z$  39) is the predominant fragment ion peak in the CID-MS/MS mass spectrum of  $[\text{Ala}+\text{K}]^+$  under “normal” ion-trapping conditions, fragment ions arising from loss of  $\text{H}_2\text{O}$  ( $m/z$  110) were observed in low abundance (Figure 1c). Characteristic fragment ions associated with the loss of  $\text{CO}$ ,  $\text{NH}_3$ , and  $(\text{CO}+\text{NH}_3)$  in  $[\text{Ala}+\text{Li}/\text{Na}]^+$  were absent. As in the case of  $[\text{Ala}/([\text{D}_3]\text{Ala})+\text{Na}]^+$ , a very minor  $[\text{K}+\text{H}_2\text{O}/\text{D}_2\text{O}]^+$  ( $m/z$  57/59) fragment ion (relative intensity ca. 0.2% of the  $\text{K}^+$  ( $m/z$  39) base peak, Figure 1c) was found, which indicates that the  $[\text{K}+\text{H}_2\text{O}/\text{D}_2\text{O}]^+$  ion is also formed directly from the dissociation of  $[\text{Ala}/([\text{D}_3]\text{Ala})+\text{K}]^+$  (see also ref. [26]).

The order of appearance threshold voltages (in V) is:  $[\text{Ala}+\text{K}]^+$ :  $\text{K}^+$  formation (0.26) <  $-\text{H}_2\text{O}$  (0.42) <  $[\text{K}+\text{H}_2\text{O}]^+$  (0.44).

Again, agreement between the order of experimental threshold voltages and theoretical critical energies of dissociation is observed (Table 2), except that, based on the energetics data presented in Table 2, loss of  $\text{NH}_3$  (with critical energy at  $158\text{ kJ mol}^{-1}$ ) should also be observed experimentally because loss of  $\text{H}_2\text{O}$  with a higher critical energy was observed. This apparent inconsistency will be discussed in detail (see section “Absence of  $\text{NH}_3$  from  $[\text{Ala}+\text{K}]^+$ ” below). Coincidentally, the loss of  $\text{CO}$  (via **21K**) and the formation of  $[\text{K}+\text{H}_2\text{O}]^+$  (via **11K**) are estimated to have a similar energy barrier of  $183\text{ kJ mol}^{-1}$  (Table 2). However, as only the latter was observed (Figure 1c), this suggests that kinetic factors could favor the formation of  $[\text{K}+\text{H}_2\text{O}]^+$ .

**Rationalization of the dissociation of  $[\text{Ala}+\text{M}]^+$ :** Our theoretical results suggest that competitive loss of neutral molecules from  $[\text{Ala}+\text{M}]^+$  ( $\text{M}^+=\text{Li}^+, \text{Na}^+, \text{K}^+$ ) occurs on potential energy surfaces consisting of very similar intermediates and transition structures, within a narrow energy window of about  $70\text{ kJ mol}^{-1}$  (Table 1). However, the relative barriers for the various dissociation channels (Table 2) are in fact dependent on the nature of the alkali metal cation. The factors governing the competitive dissociation of  $[\text{Ala}+\text{M}]^+$  are discussed in detail below

**Formation of  $\text{M}^+$ :** As discussed above, formation of  $\text{M}^+$  is absent in  $[\text{Ala}+\text{Li}]^+$ , but is observed as a major channel in  $[\text{Ala}+\text{Na}]^+$  and  $[\text{Ala}+\text{K}]^+$ . This clearly reflects the weaker  $\text{M}^+$  binding affinity of Ala with increasing ionic size, in the order  $\text{Li}^+ > \text{Na}^+ > \text{K}^+$ .<sup>[15e,f,16a]</sup> As a result, for the smallest cation  $\text{Li}^+$ , the Ala binding affinity ( $251\text{ kJ mol}^{-1}$ ) is significantly higher (by  $45\text{--}74\text{ kJ mol}^{-1}$ , Table 2) than the critical energies of the dissociation channels leading to the loss of small neutrals. For the largest cation  $\text{K}^+$ , the Ala affinity ( $123\text{ kJ mol}^{-1}$ ) is significantly lower (by  $42\text{--}60\text{ kJ mol}^{-1}$ , Table 2). For  $\text{Na}^+$ , the Ala affinity ( $174\text{ kJ mol}^{-1}$ ) lies about halfway between the narrow range (ca.  $11\text{ kJ mol}^{-1}$ ) of critical energies for the other dissociation pathways (Table 2). Thus, the formation of  $\text{Na}^+$  was observed in competition

with the loss of neutrals such as  $\text{CO}$ ,  $\text{H}_2\text{O}$ , and  $\text{NH}_3$  in  $[\text{Ala}+\text{Na}]^+$ .

**Formation of  $[\text{M}+\text{H}_2\text{O}]^+$  ( $\text{M}=\text{Na}^+$  and  $\text{K}^+$ ):** As discussed above and depicted in Figure 3, ion–molecule complex **9Li** can lead to the formation of two sets of products, which differ in the ligand (2-iminopropanal versus water) to which  $\text{Li}^+$  is bound. For all three alkali metal cations, binding to 2-iminopropanal is preferred, so that formation of metal-bound 2-iminopropanal (**10**) and loss of water is favored. What differs between the three alkali cations is that for  $\text{Na}^+$  and  $\text{K}^+$  (but not for  $\text{Li}^+$ ),  $[\text{M}+\text{H}_2\text{O}]^+$  is also observed as a minor fragment. In the case of  $\text{Li}^+$  (Figure 3), we already noted that the energy of the transition structure **6Li** is lower (by ca.  $30\text{ kJ mol}^{-1}$ ) than that of 2-iminopropanal + **13Li** (lithiated water). As a result, lithiated alanine molecules which have surmounted barrier **6Li** (which yields **10Li** +  $\text{H}_2\text{O}$  eventually), do not necessarily have enough energy to form 2-iminopropanal + **13Li**. For sodium, the stability of barrier **6Na** is comparable to that of 2-iminopropanal + **13Na**, while for potassium, barrier **6K** becomes higher (by ca.  $15\text{ kJ mol}^{-1}$ ) than 2-iminopropanal + **13K**, and this suggests that for  $\text{Na}^+$  and  $\text{K}^+$ , the formation of a minor metal-cation-bound water fragment ion  $[\text{Na/K}+\text{H}_2\text{O}]^+$  would be plausible. This is in fact consistent with our experimental findings.

**Absence of  $\text{NH}_3$  from  $[\text{Ala}+\text{K}]^+$ :** Interestingly, for  $[\text{Ala}+\text{K}]^+$ , even though the energetic requirement for loss of  $\text{NH}_3$  (via **19K**) is lower than that for  $\text{H}_2\text{O}$  (via **6K**) by  $7\text{ kJ mol}^{-1}$  (Table 2), the loss of ammonia was not observed under ion-trap CID conditions, while the peak due to loss of  $\text{H}_2\text{O}$  was clearly visible over a relatively wide range of collision energies above the threshold voltage (Figure 2c). Given the general agreement between experiment and theory, this inconsistency is in fact puzzling. After careful inspection of the potential energy surface, we offer the following plausible explanation: the absence of  $\text{NH}_3$  in  $[\text{Ala}+\text{K}]^+$  probably arises from the stability of species **18K** (a  $\text{NH}_3\cdots\text{methyloxiranone}\cdots\text{K}^+$  ion–molecule intermediate) and the instability of species **21K** (a  $\text{NH}_3\cdots\text{K}^+\cdots\text{methyloxiranone}$  ion–molecule transition structure).

As discussed earlier, the pathway for loss of  $\text{NH}_3$  shares some of the intermediate and transition structures of the pathway leading to the loss of  $\text{CO}$  and  $(\text{CO}+\text{NH}_3)$  (Figure 3). The ion–molecule intermediate **18** may lose  $\text{NH}_3$  by direct bond fission with formation of the  $[\text{Ala}+\text{M}-\text{NH}_3]^+$  fragment ion (species **19**), an alkaliated methyloxiranone. Alternatively, the intermediate **18** may rearrange to the thermodynamically more stable intermediate **20** (as illustrated in Scheme 2). For species **20** to react further, it must surmount the energy barrier of transition structure **21** to eventually yield  $\text{CO}$  or  $(\text{CO}+\text{NH}_3)$ . Of the three  $[\text{Ala}+\text{Li}/\text{Na}/\text{K}]^+$  systems, species **18** is most stable in the case of potassium (**18Li**, **18Na**, and **18K** lie 177, 155, and  $136\text{ kJ mol}^{-1}$ , respectively, above the corresponding species **1**, Figure 3). On the other hand, species **21** is most unstable



in  $[\text{Ala}+\text{K}]^+$  (**21Li**, **21Na**, and **21K** lie 152, 170, and 183  $\text{kJ mol}^{-1}$ , respectively, above the corresponding species **1**). Thus, what may be happening under the CID conditions of the ion trap is that the presence of a particularly stable **18K** diverts the reaction away from loss of  $\text{NH}_3$  to formation of species **20K**. In other words, we speculate that because of the relatively stable **18K** and unstable **21K**, if the dissociating  $[\text{Ala}+\text{M}]^+$  samples this part of the potential energy surface, it would end up “trapped” as the intermediate species **20K** instead of losing  $\text{NH}_3$  as expected. We note that a barrier of 183  $\text{kJ mol}^{-1}$  must be surmounted if loss of  $\text{NH}_3$  is to occur from species **21K**. As this is some 20  $\text{kJ mol}^{-1}$  higher than the barrier for the pathway for loss of  $\text{H}_2\text{O}$  (via transition structure **6K**), this may explain why loss of  $\text{H}_2\text{O}$  but not  $\text{NH}_3$  was observed in the ion-trap CID-MS/MS spectrum of  $[\text{Ala}+\text{K}]^+$ .<sup>[27]</sup>

**Compression/expansion of potential energy surface:** Unlike the loss of CO versus  $(\text{CO}+\text{NH}_3)$ , losses of  $\text{H}_2\text{O}$  and  $\text{NH}_3$  derive from different transition structures (via species **6** and **19**, respectively). Here we note that the relative energy barrier for the loss of  $\text{H}_2\text{O}$  (via **6**) and  $\text{NH}_3$  (via **19**) decreases from 24 ( $\text{Li}^+$ ) to 5 ( $\text{Na}^+$ ) to  $-7 \text{ kJ mol}^{-1}$  ( $\text{K}^+$ ), that is, the loss of  $\text{H}_2\text{O}$  becomes kinetically less favorable with increasing ionic size.

On further examination of the energetics of various species on the potential energy surface, one finds interesting variation in the energies from one cation to another (depicted graphically in Figure 5, based on values summarized in Table 1). For most species on the potential energy surface, from  $\text{K}^+$  to  $\text{Na}^+$  to  $\text{Li}^+$ , the surface has expanded, that is, it is relatively less stable (compared to **1**) for most species to be in these forms when the cation is small. For a few species on the potential energy surface (**7**, **20**, **21**, **22**, and **23**),<sup>[28]</sup> from  $\text{K}^+$  to  $\text{Na}^+$  to  $\text{Li}^+$ , the surface is compressed, that is, it is relatively more stable (compared to **1**) for these species to be in these forms when the cation is small. We note that for these species, an “ion-cluster” type of geometry is adopted, that is,  $\text{M}^+$  interacts with more than one ligand.

We propose the following explanation for the observed trends. In alanine, there are three potential metal cation binding sites: amino nitrogen ( $\text{NH}_2$ ), carbonyl oxygen ( $\text{O}=\text{C}$ ), and hydroxyl oxygen ( $\text{OH}$ ). When the ligand is “intact”, the positions of these three sites are constrained by the covalent bonds in the ligand. For example, as long as the carboxyl group ( $\text{COOH}$ ) is retained (e.g., in **1–4**), the two oxygen atoms would be approximately 2–3 Å from each other. Therefore, it is unlikely that the metal cation could interact with individual basic sites in the optimal fashion. On the potential energy surface, species **1** exhibits the best mode of binding (in terms of energy) between  $\text{M}^+$  and an intact ligand. Given the geometrical constraints, any configuration other than that adopted in **1** would be higher in energy. Among the three cations, the  $\text{Li}^+$ –ligand interaction is the strongest. Thus, by adopting any other configuration, species on the  $[\text{Ala}+\text{Li}]^+$  potential energy surface will be relatively less stable when compared to the corresponding

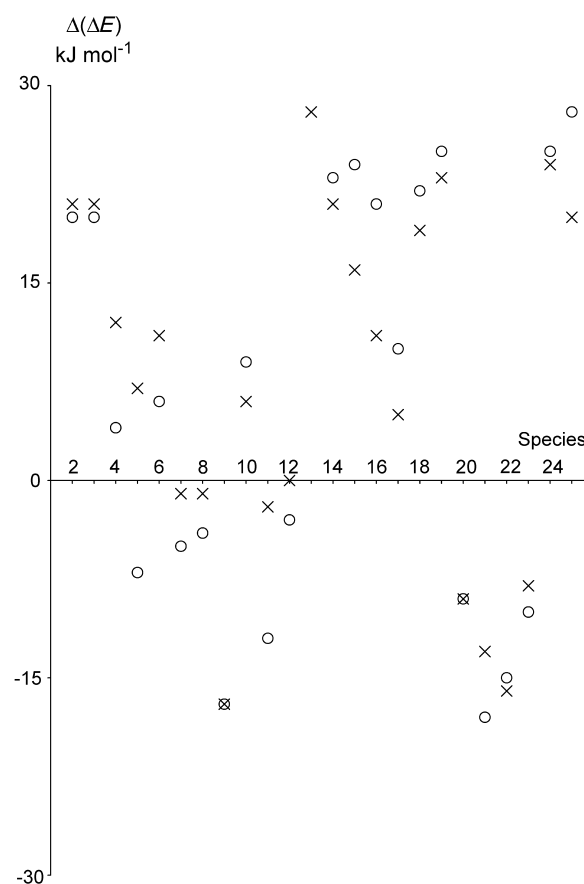


Figure 5. Variation of relative energies  $\Delta(\Delta E)$  of various species (with respect to **1**) on the  $[\text{Ala}+\text{M}]^+$  potential energy surface: from  $\text{K}^+$  to  $\text{Na}^+$  as  $\times$  and  $\text{Na}^+$  to  $\text{Li}^+$  as  $\circ$ . A positive value suggests an expansion of potential energy with smaller cation size.

species on the  $[\text{Ala}+\text{K}]^+$  surface; that is, the potential energy surface would appear to be expanded for the smaller cation.

On the other hand, when the alanine ligand “breaks up”, the individual basic sites now have the opportunity to rearrange to a more optimal fashion. As an example, the two oxygen atoms in species **22** are now at least 4 Å apart (4.45, 4.93, and 5.86 Å in **22Li**, **22Na**, and **22K**, respectively). Without the geometrical constraints which are present in a single ligand, the individual binding sites on various ligands can be positioned to gain maximal interaction with the metal cation. As the  $\text{Li}^+$ –ligand interaction is the strongest, by adopting these “ion-cluster” configurations, the species will be relatively more stable when compared to species **1** on the  $[\text{Ala}+\text{K}]^+$  surface, that is, the potential energy surface would appear to be compressed for the smaller cation. The issue of nonoptimal binding has been discussed previously by Rodgers and Armentrout: while one [12]crown-4 molecule has the same number of oxygen atoms as four molecules of dimethyl ether, the  $\text{M}^+$  affinity is substantially lower for the crown ether.<sup>[29]</sup> However, as far as we are aware, it is the first time that such concepts have been invoked to explain the variation of energies as a function of

cation size on the potential energy surface of dissociation processes.

Given the above, one can view the entire potential energy surface for the  $[\text{Ala}+\text{M}]^+$  dissociation as a fusion of two types of systems with difference dependences on cation size. With decreasing ionic size: 1) if  $\text{M}^+$  binds to a single ligand, the surface would be expanded; and 2) if  $\text{M}^+$  binds to more than one ligands, the surface would be compressed.

Thus, the key barrier to the loss of  $\text{H}_2\text{O}$  (species **6**) increases from  $\text{K}^+$  to  $\text{Li}^+$ , as only one ligand is involved in binding of  $\text{M}^+$ . However, for the loss of  $\text{CO}$  and  $(\text{CO}+\text{NH}_3)$ , the key barrier **21** adopts an ion-cluster type geometry, and thus the barrier decreases from  $\text{K}^+$  to  $\text{Li}^+$ . As a result of this change in relative stabilities, while barrier **6** is higher than **21** for  $[\text{Ala}+\text{Li}]^+$ , the reverse is true for  $[\text{Ala}+\text{K}]^+$ , and this results in the absence of  $(\text{CO}+\text{NH}_3)$  for  $[\text{Ala}+\text{K}]^+$ . Thus, even though absolute  $\text{M}^+$  affinities always decrease with increasing ionic size,<sup>[15c, f, 16a]</sup> the metal cation changes the relative energetics of various species on the potential energy surface, which in turn may change the preferred dissociation pathway for loss of different small neutral molecules.

**Dissociation of free versus alkaliated alanine:** We now discuss the loss of small neutral molecules from the free alanine molecule, not bound to any metal cation. By comparing the dissociation of free alanine with that of alkaliated alanine, the role of the cation in the dissociation of  $[\text{Ala}+\text{M}]^+$  can be elucidated.

It is clear that in the absence of  $\text{M}^+$ , formation of ion-molecule complexes such as **20**, **21**, **22**, and so on (Figure 4) is not possible. Thus, if loss of  $\text{CO}$  and  $(\text{CO}+\text{NH}_3)$  are to occur from free alanine, the mechanism would have to be different to that proposed for alkaliated alanine, possibly with a much higher energy barrier.

One key to the loss of  $\text{NH}_3$  is the formation of the zwitterionic species **17**. The most important distinction between the  $[\text{Ala}+\text{M}]^+$  and Ala potential energy surface is that without  $\text{M}^+$ , zwitterionic minimum **17** (and the associated transition structure **16**) cannot be located. To verify whether it is a computational artifact, we carried out optimization of species **17** at other levels of theory (larger basis set, with diffuse and polarization function, and at the MP2 level). Again, the analogous species **17** cannot be located on the free-Ala potential energy surface. Based on the above, the presence of a cation is important in stabilization of the zwitterionic form of alanine, similar to what was found for glycine previously,<sup>[30]</sup> and this suggests that the presence of  $\text{M}^+$  is crucial in the loss of  $\text{NH}_3$  from alkaliated aliphatic amino acids.

For the loss of  $\text{H}_2\text{O}$ , we carried out the corresponding theoretical study for the dissociation of free alanine. The structures of species involved in the loss of  $\text{H}_2\text{O}$  from free alanine (Figure 6) are in general very similar to that presented for  $[\text{Ala}+\text{M}]^+$  (Figure 4), but with  $\text{M}^+$  removed. To facilitate discussion, we named the analogous species in free-alanine dissociation to those found for  $[\text{Ala}+\text{M}]^+$  with the same number, suffixed by "L", that is, **1L**, **2L**, **3L**, and so

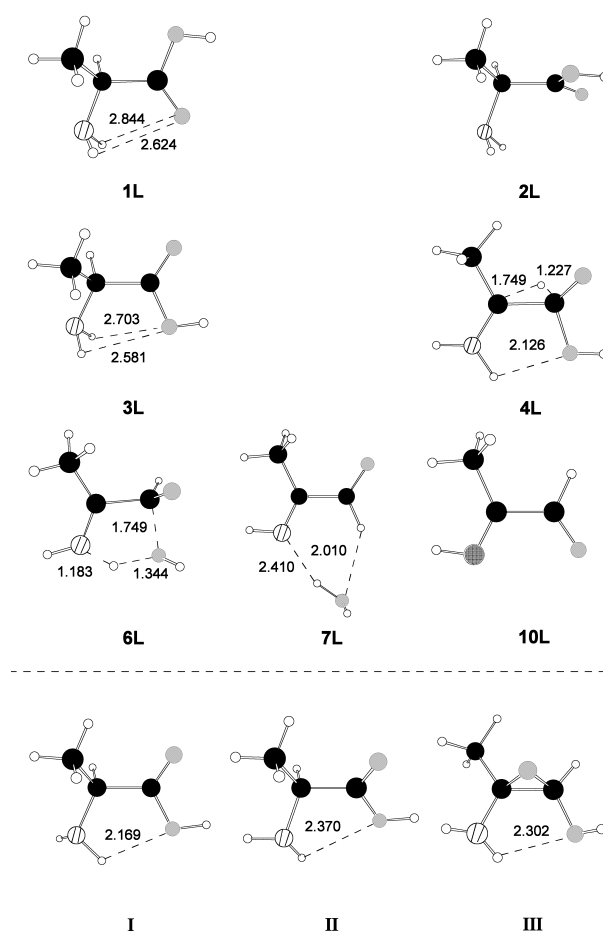


Figure 6. Optimized structures for the loss of  $\text{H}_2\text{O}$  from free Ala. The species analogous to those found for  $[\text{Ala}+\text{M}]^+$  are denoted with the same number suffixed by "L", that is, **1L**, **2L**, **3L**, etc. for the counterparts of species **1**, **2**, **3**, etc. for  $[\text{Ala}+\text{M}]^+$ . The three species on the free alanine surface that are not analogous to those found in  $[\text{Ala}+\text{M}]^+$  are denoted as **I**, **II**, and **III**.

on, for the corresponding species **1**, **2**, **3**, and so on, for  $[\text{Ala}+\text{M}]^+$ .

Although the binding of  $\text{M}^+$  to alanine is largely electrostatic, the presence of a metal cation generally weakens the covalent bond in the ligand in proximity to the cation-binding site. For example, the bond order of the carbonyl bond is closer to a  $\text{C}=\text{O}$  bond in the free ligand **2L** (estimated bond order ca. 1.8) than in the lithiated complex **2Li** (estimated bond order ca. 1.5). What is more interesting is that complexation with alkali metal cations may stabilize or destabilize various forms of the ligand (Figure 7): while species **2L** and **3L** are destabilized, the others (**4L** to **10L**) are stabilized in the presence of the alkali metal cation. We believe that two factors are at work here: the number of interactions (denticity) between the cation and ligand, and the magnitude of charge separation in the ligand (dipole moment). For **1L**, **2L**, and **3L**, the dipole moments of the ligands are quite similar in these three forms (1.4–1.7 D), so losing one  $\text{M}^+\cdots\text{N}$  interaction in **2L** and **3L** leads to an energy penalty of at least  $65\text{ kJ mol}^{-1}$ . On the other hand,

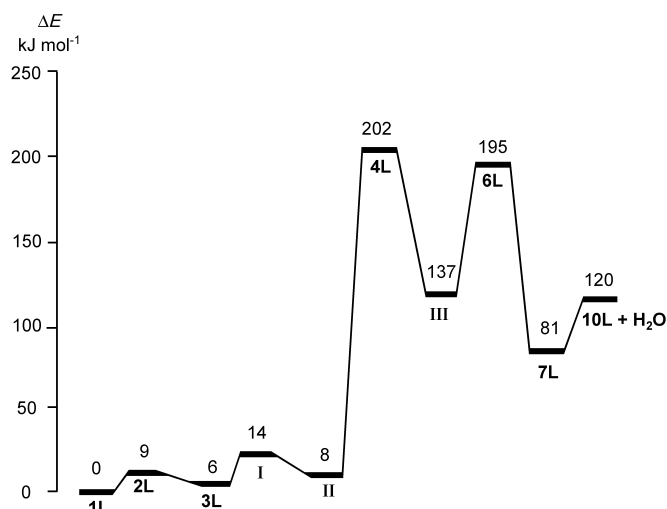


Figure 7. Potential energy surface for the loss of  $\text{H}_2\text{O}$  from free Ala. The species analogous to those found for  $[\text{Ala}+\text{M}]^+$  are denoted with the same number, suffixed by “L”, that is, **1L**, **2L**, **3L**, etc. for the counterpart of species **1**, **2**, **3** etc. for the  $[\text{Ala}+\text{M}]^+$ . The three species on the free alanine surface that are not analogous to those found in  $[\text{Ala}+\text{M}]^+$  are denoted as **I**, **II**, and **III**.

the dipole moment of species **4L** to **10L** ranges from 4.2 to 6.4 D, which is much larger than that of **1L** (1.4 D). Hence, the stabilizing effect of a cation “solvating” the ligand would be more strongly felt in a more polar ligand.<sup>[8]</sup> In this case, as the key transition structures (**4L** and **6L**) are more polar than **1L** in Ala, the corresponding barriers in  $[\text{Ala}+\text{M}]^+$  (**4** and **6**) are lowered when compared to that of Ala.

## Conclusion

Dissociation of alkaliated alanine  $[\text{Ala}+\text{M}]^+$  ( $\text{M}^+=\text{Li}^+$ ,  $\text{Na}^+$ ,  $\text{K}^+$ ) with formation of  $\text{M}^+$  and loss of small stable neutral molecules [ $\text{H}_2\text{O}$ ,  $\text{CO}$ ,  $\text{NH}_3$  and  $(\text{CO}+\text{NH}_3)$ ] has been studied by low-energy ion-trap CID tandem mass spectrometry and density functional theory. The order of threshold voltages (critical energy) for different dissociation pathways obtained experimentally was found to be consistent with the order of critical energies (energy barriers) on the potential energy surface obtained theoretically, and thus the necessary confidence in both the experimental and theoretical results is provided.

Owing to proton deficiency,  $[\text{Ala}+\text{M}]^+$  lose small stable neutrals with totally different mechanisms than  $[\text{Ala}+\text{H}]^+$ . Although not explicitly involved in dissociation, the alkali metal cation plays several important roles:

- 1) It facilitates the formation of amino acids in the zwitterionic form and thus promotes the loss of  $\text{NH}_3$  and related fragments from alkaliated amino acids.
- 2) It lowers the dissociation barrier by preferentially stabilizing the more polar transition structures and thus effectively catalyzes the different dissociation pathways.

- 3) It acts as an anchor point for small neutral molecules and thus leads to the formation of stable but loosely bound ion–molecule complexes and lowers the energy requirement for dissociation.
- 4) It changes the relative energy barriers of the potential energy surface for competing dissociation pathway of  $[\text{Ala}+\text{M}]^+$  and results in changes in the energetically preferred dissociation channels for amino acids cationized by different alkali metal cations.

## Experimental and Theoretical Section

**Experimental details:** Chemicals, including ( $[\text{D}_3]$ methyl)alanine,  $\text{D}_2\text{O}$ , and  $\text{CH}_3\text{OD}$ , were purchased from Sigma-Aldrich Chemicals (St. Louis, USA) and were used as received. The solvents were purchased from Mallinckrodt (Paris, Kentucky, USA). Sample solutions were prepared by dissolving  $\text{KNO}_3/\text{NaNO}_3/\text{LiNO}_3$  and alanine (final concentration each of  $10^{-4} \text{ mol L}^{-1}$ ) in  $\text{MeOH}/\text{H}_2\text{O}$  (50/50, v/v). The sample solutions for H/D exchange and deuterium-labeling studies were prepared in the same way as those for standard experiments, except for replacing  $\text{H}_2\text{O}/\text{MeOH}$  with  $\text{D}_2\text{O}/\text{CH}_3\text{OD}$  as the solvent, or alanine with ( $[\text{D}_3]$ methyl)alanine ( $\text{NH}_2\text{CH}(\text{CD}_3)\text{COOH}$ ).

Low-energy CID-MS/MS mass spectra of alkaliated alanine,  $[\text{Ala}+\text{M}]^+$ , were recorded with a Finnigan-LCO quadrupole ion-trap mass analyzer (San Jose, USA) equipped with an electrospray ionization (ESI) interface and controlled via the Xcalibur (Version 1.2) system software.<sup>[31]</sup> The sample solution was introduced into the ESI interface by a syringe pump (Harvard Apparatus, Model 22) at  $3\text{--}4 \mu\text{L min}^{-1}$ . The ESI spray voltage was set at 4–4.5 kV, and the temperature of the heated capillary was 120–150 °C. Nitrogen sheath gas was supplied at  $60 \text{ Lh}^{-1}$  to assist solvent evaporation. The mass analyzer was operated in the low-mass scan mode: the main radio-frequency (RF) voltage applied to the ring electrode during the ion-injection step was reduced from the standard 400–250 to 250–200 V ( $V_{\text{p-p}}$ ) range to optimize trapped ion intensities for ions with  $m/z$  values below 200. In practice, the main RF voltage of the ring electrode was optimized (adjusted) via the Xcalibur software at a  $m/z$  value midway between three units higher (arbitrarily chosen) than that of the precursor  $[\text{Ala}+\text{M}]^+$  ( $\text{M}^+=\text{Li}^+$ ,  $\text{Na}^+$ ,  $\text{K}^+$ ) ion and the default value of 30. The trap offset voltage was set in the range of  $-5$  to  $-10$  V. These conditions led to the formation of a moderately intense alkaliated alanine precursor ion  $[\text{Ala}+\text{M}]^+$  (with ion injection time of 25–70 ms, and  $1.5\text{--}3.0 \times 10^5$  ion intensity units as displayed by the Xcalibur (Version 1.2) system software at the ion-detector setting of 1000 V), which was isolated by ejecting all other ions from the trap (isolation width of 1–3  $m/z$  values). Collision-induced dissociation of the isolated  $[\text{Ala}+\text{M}]^+$  ions with the helium buffer gas (ca. 1 mTorr pressure) in the ion trap was achieved by applying and varying an auxiliary ion activation RF voltage to the end-cap electrodes in the range of 0.1–0.6 V in 0.01 V increments, with ion activation  $q_z$  in the range of 0.2 to 0.3 and activation time of 3–10 ms.<sup>[31]</sup> The fragment ions resulting from the CID processes, i.e., the MS/MS spectra, were recorded by scanning the ion-trap mass analyzer from the  $m/z$  of  $[\text{Ala}+\text{M}]^+$  down to  $m/z$  20. Usually, a mass spectrum was obtained by averaging 50 scans, with relative ion intensities reproducible to  $\pm 8\%$ . We attempted to obtain the CID-MS/MS spectra of the fragment ions, i.e.,  $\text{MS}^3$  studies on the isolated  $[\text{Ala}+\text{M}]^+$  ions, but failed due to the instability of the ion-trap analyzer in the  $\text{MS}^3$  mode of operation in the low- $m/z$  region.

The identities of the fragment ions formed and neutrals lost were confirmed by accurate mass measurements with a Micromass quadrupole time-of-flight (Q-TOF II) tandem mass spectrometer (Manchester, UK) equipped with an ESI interface. The absence of  $\text{Li}^+$  ion formation in the dissociation of  $[\text{Ala}+\text{Li}]^+$  was confirmed by the CID-MS/MS spectrum recorded with a Micromass Quattro Ultima triple-quadrupole tandem

mass spectrometer (Manchester, UK) capable of detecting ions with  $m/z$  values as low as  $\text{He}^+$  ( $m/z$  4).

**Computational methods:** Density functional calculations were performed with the Gaussian98 package.<sup>[32]</sup> All structures were fully optimized at the B3LYP/6-31G(d) level, and the nature of stationary points was confirmed by frequency calculation, with transition structures verified to be connecting the specific minima by intrinsic reaction coordinate (IRC) calculations. With these structures, single-point energy calculations were performed at the B3LYP/6-311+G(3df,2p) level. The electronic energies at 0 K of all species were corrected with B3LYP/6-31G(d) zero-point vibrational energies, scaled by 0.9806.<sup>[33]</sup> Charge and bond order were analyzed by using the natural bond orbital (NBO) scheme for selected species at the B3LYP/6-31G(d) level.<sup>[34]</sup>

Our choice of the B3LYP functional is justified as it has been shown that it yields accurate  $\text{Li}^{+25}$  and  $\text{K}^{+35}$  binding affinities for a wide range of ligands at a computationally affordable cost. Furthermore, this functional has been successfully applied to elucidate the dissociation mechanism of several cationized amino acid systems.<sup>[10,11b,12a,12c,12d]</sup> We note here that we have not included basis-set superposition error (BSSE) in our model, as it has been found that at this level, counterpoise correction tends to be small.<sup>[35]</sup> Moreover, as the correction is expected to be uniform, it would have little impact on the shape of the potential energy surface we presented.

## Acknowledgements

The generous allocation of supercomputer time and the award of a postgraduate studentship from the Institute of High Performance Computing to S.A. are gratefully acknowledged. The funding support of the Hong Kong University to C.C.L.W., and of the Hong Kong Polytechnic University (Area of Strategic Development Fund Project No. A024) and the Research Grant Council of Hong Kong (Area of Excellence Project No. P-10/2001 and CERG Project No. PolyU 5286/02P) to C.W.T. are gratefully acknowledged. The involvement of Mr. J. K. C. Lau in the early stage of the project and Ms. Carrie H. S. Wong in preparing this manuscript are also appreciated.

- [1] a) J. R. Yates, *J. Mass Spectrom.* **1998**, *33*, 1; b) J. Rappsilber, M. Moniatte, M. L. Nielsen, A. V. Podtelejnikov, M. Mann, *Int. J. Mass Spectrom.* **2003**, *226*, 223; c) R. Aebersold, M. Mann, *Nature* **2003**, *422*, 198; d) J. R. Yates, *Annu. Rev. Biophys. Biomol. Struct.* **2004**, *33*, 297.
- [2] a) A. R. Dongre, J. L. Jones, A. Somogyi, V. H. Wysocki, *J. Am. Chem. Soc.* **1996**, *118*, 8365; b) V. H. Wysocki, G. Tsaprailis, L. L. Smith, L. A. Breci, *J. Mass Spectrom.* **2000**, *35*, 1399.
- [3] a) L. M. Mallis, D. H. Russell, *Anal. Chem.* **1986**, *58*, 1067; b) D. H. Russell, E. S. McGlohon, L. M. Mallis, *Anal. Chem.* **1988**, *60*, 1818; c) X. Tang, W. Ens, K. G. Standing, J. W. Westmore, *Anal. Chem.* **1988**, *60*, 1791.
- [4] a) J. Adams, M. L. Gross, *J. Am. Chem. Soc.* **1986**, *108*, 6915; b) J. Adams, M. L. Gross, *Anal. Chem.* **1987**, *59*, 1576; c) R. P. Grese, R. L. Cerny, M. L. Gross, *J. Am. Chem. Soc.* **1989**, *111*, 2835; d) R. P. Grese, M. L. Gross, *J. Am. Chem. Soc.* **1990**, *112*, 5098; e) L. M. Teesch, R. C. Orlando, J. Adams, *J. Am. Chem. Soc.* **1991**, *113*, 812; f) L. M. Teesch, R. C. Orlando, J. Adams, *J. Am. Chem. Soc.* **1991**, *113*, 3668.
- [5] a) J. A. Leary, T. D. Williams, G. Bott, *Rapid Commun. Mass Spectrom.* **1989**, *3*, 192; b) J. A. Leary, Z. Zhou, S. A. Ogden, T. D. Williams, *J. Am. Soc. Mass Spectrom.* **1990**, *1*, 473.
- [6] a) T. Lin, G. L. Glish, *Anal. Chem.* **1998**, *70*, 5162; b) T. Lin, A. H. Payne, G. L. Glish, *J. Am. Soc. Mass Spectrom.* **2001**, *12*, 497.
- [7] M. M. Kish, C. Wesdemiotis, *Int. J. Mass Spectrom.* **2003**, *227*, 191.
- [8] W. Y. Feng, C. Gronert, K. A. Fletcher, A. Warres, C. B. Lebrilla, *Int. J. Mass Spectrom.* **2003**, *222*, 117.
- [9] a) E. Uggerud, *Theor. Chem. Acc.* **1997**, *97*, 313; b) R. A. J. O'Hair, P. S. Broughton, M. L. Styles, B. T. Frink, C. M. Hadad, *J. Am. Soc. Mass Spectrom.* **2000**, *11*, 687; c) F. Rogalewicz, Y. Hoppilliard, G. Ohanessian, *Int. J. Mass Spectrom.* **2000**, *195*, 565; d) F. Rogalewicz, Y. Hoppilliard, *Int. J. Mass Spectrom.* **2000**, *199*, 235.
- [10] L. Rodriguez-Santiago, M. Sodupe, J. Tortajada, *J. Phys. Chem. A* **2001**, *105*, 5340.
- [11] a) H. Lavanant, Y. Hoppilliard, *J. Mass Spectrom.* **1997**, *32*, 1037; b) Y. Hoppilliard, G. Ohanessian, S. Bourcier, *J. Phys. Chem. A* **2004**, *108*, 9687.
- [12] a) T. Shoeib, A. C. Hopkinson, K. W. M. Siu, *J. Phys. Chem. B* **2001**, *105*, 12399; b) E. R. Talaty, B. A. Perera, A. L. Gallardo, J. M. Barr, M. J. Van Stipdonk, *J. Phys. Chem. A* **2001**, *105*, 8059; c) T. Shoeib, A. Cunje, A. C. Hopkinson, K. W. M. Siu, *J. Am. Soc. Mass Spectrom.* **2002**, *13*, 408; d) D. Caraiman, T. Shoeib, K. W. M. Siu, A. C. Hopkinson, D. K. Bohme, *Int. J. Mass Spectrom.* **2003**, *228*, 629.
- [13] a) F. Rogalewicz, Y. Hoppilliard, G. Ohanessian, *Int. J. Mass Spectrom.* **2000**, *201*, 307; b) Y. Hoppilliard, F. Rogalewicz, G. Ohanessian, *Int. J. Mass Spectrom.* **2001**, *204*, 267; c) F. Rogalewicz, Y. Hoppilliard, G. Ohanessian, *Int. J. Mass Spectrom.* **2001**, *206*, 45.
- [14] K. Eller, H. Schwarz, *Chem. Rev.* **1991**, *91*, 1121.
- [15] a) R. A. Jockusch, W. D. Price, E. R. Williams, *J. Phys. Chem. A* **1999**, *103*, 9266; b) E. F. Strittmatter, A. S. Lemoff, E. R. Williams, *J. Phys. Chem. A* **2000**, *104*, 9793; c) B. Balta, M. Basma, V. Aviyente, C. B. Zhu, C. Lifshitz, *Int. J. Mass Spectrom.* **2000**, *201*, 69; d) S. Pulkkinen, M. Noguera, L. Rodriguez-Santiago, M. Sodupe, J. Bertran, *Chem. Eur. J.* **2000**, *6*, 4393; e) T. Marino, N. Russo, M. Toscano, *J. Inorg. Biochem.* **2000**, *79*, 179; f) T. Marino, N. Russo, M. Toscano, *Inorg. Chem.* **2001**, *40*, 6439; g) S. Hoyau, J. P. Pelicier, F. Rogalewicz, Y. Hoppilliard, G. Ohanessian, *Eur. J. Mass Spectrom.* **2001**, *7*, 303; h) R. C. Dunbar, *J. Phys. Chem.* **2000**, *104*, 8067; i) A. Gapeev, R. C. Dunbar, *J. Am. Chem. Soc.* **2001**, *123*, 8360; j) C. H. S. Wong, F. M. Siu, N. L. Ma, C. W. Tsang, *J. Mol. Struct.* **2002**, *588*, 9; k) R. M. Moision, P. B. Armentrout, *J. Phys. Chem. A* **2002**, *106*, 10350; l) J. M. Talley, B. A. Cerda, G. Ohanessian, C. Wesdemiotis, *Chem. Eur. J.* **2002**, *8*, 1377; m) C. Kapota, J. Lemaire, P. Maitre, G. Ohanessian, *J. Am. Chem. Soc.* **2004**, *126*, 1836; n) F. M. Siu, N. L. Ma, C. W. Tsang, *Chem. Eur. J.* **2004**, *10*, 1966; o) R. M. Moision, P. B. Armentrout, *Phys. Chem. Chem. Phys.* **2004**, *6*, 2588.
- [16] a) S. Hoyau, G. Ohanessian, *Chem. Eur. J.* **1998**, *4*, 1561; b) T. Marino, N. Russo, M. Toscano, *J. Phys. Chem. B* **2003**, *107*, 2588.
- [17] T. Fujii, *Mass Spectrom. Rev.* **2000**, *19*, 111.
- [18] a) J. S. Brodbelt, H. I. Kenttamaa, R. G. Cooks, *Org. Mass Spectrom.* **1988**, *23*, 6; b) J. Gronowska, C. Paradisi, P. Traldi, U. Vettori, *Rapid Commun. Mass Spectrom.* **1990**, *4*, 306.
- [19] C. Lifshitz, *Eur. J. Mass Spectrom.* **2002**, *8*, 85.
- [20] K. J. Hart, S. A. McLuckey, *J. Am. Soc. Mass Spectrom.* **1994**, *5*, 250.
- [21] A. Colorado, J. Brodbelt, *J. Am. Soc. Mass Spectrom.* **1996**, *7*, 1116.
- [22] This work. Our calculated  $\text{Li}^+$  affinities (at 0 K) for CO and  $\text{NH}_3$  are 66 and 159  $\text{kJ mol}^{-1}$ , respectively. They are in good agreement with the experimental  $\Delta H_0$  of ( $\text{Li}^+\text{-CO}$ ) of 55  $\text{kJ mol}^{-1}$  reported in ref. [23] and the experimental  $\Delta H_0$  of ( $\text{Li}^+\text{-NH}_3$ ) of 159  $\text{kJ mol}^{-1}$  (corrected from experimental  $\Delta H_{298}(\text{Li}^+\text{-NH}_3)=164 \text{ kJ mol}^{-1}$ ) reported in ref. [24] and 160  $\text{kJ mol}^{-1}$  (corrected from experimental  $\Delta G_{373}=30.2 \text{ kcal mol}^{-1}$ ) reported in ref. [25a].
- [23] D. Walter, M. R. Sievers, O. B. Armentrout, *Int. J. Mass Spectrom. Ion Processes* **1998**, *175*, 93.
- [24] R. L. Woodin, J. L. Beauchamp, *J. Am. Chem. Soc.* **1978**, *100*, 501.
- [25] a) P. Burk, I. A. Koppel, I. Koppel, R. Kurg, J.-F. Gal, P.-C. Maria, M. Herreros, R. Notario, J.-L. M. Abbound, F. Anvia and R. W. Taft, *J. Phys. Chem. A* **2000**, *104*, 2824; b) R. W. Taft, F. Anvia, J.-F. Gal, S. Walsh, M. Capon, M. C. Holmes, K. Hosn, G. Oloumi, R. Vasanwala and S. Yazdani, *Pure Appl. Chem.* **1990**, *62*, 17.
- [26] As  $\text{K}^+$  is present in high abundance in the MS/MS spectrum of  $[\text{Ala}+\text{K}]^+$  (Figure 1c), the  $[\text{K}+\text{H}_2\text{O}]^+$  ion may also be formed by further reaction of  $\text{K}^+$  with background moisture ( $\text{H}_2\text{O}$ ) or water adsorbed on the wall of the ring/end-cap electrodes of the unheated ion-trap mass analyzer. However, only a very low intensity  $[\text{K}+\text{D}_2\text{O}]^+$  peak (but no  $[\text{K}+\text{H}_2\text{O}]^+$  or  $[\text{K}+\text{HDO}]^+$ ) was observed

- in the MS/MS scans of ESI-generated potassium-cationized [D<sub>3</sub>]alanine (ND<sub>2</sub>CH(CH<sub>3</sub>)COOD). This indicates that under the ion-trap CID conditions adopted in the present study, formation of [K+H<sub>2</sub>O]<sup>+</sup> due to further reaction of K<sup>+</sup> with background/ion-trap moisture did not occur to any noticeable extent.
- [27] The rationale proposed here does not preclude the occurrence and observation of the loss-of-NH<sub>3</sub> pathway under the more energetic ionization/CID conditions and microsecond timeframe of other types of tandem mass spectrometers. Indeed, we found both the [Ala+K-H<sub>2</sub>O]<sup>+</sup> and [Ala+K-NH<sub>3</sub>]<sup>+</sup> peaks in relatively low intensities in the fast atom bombardment (FAB)/mass-analyzed ion kinetic energy (MIKE) mass spectrum obtained with a B-E sector mass spectrometer, as well as in the CID-MS/MS spectrum obtained with a triple-quadrupole mass spectrometer.
- [28] An exception is noted for species **5**. The expected expansion in potential energy surface is observed for K<sup>+</sup> to Na<sup>+</sup>, with an increase in relative affinity by 7 kJ mol<sup>-1</sup>. However, from Na<sup>+</sup> to Li<sup>+</sup>, the relative affinity decreases by 7 kJ mol<sup>-1</sup>. The origin of this abnormality is not clear, but we note that the C<sub>α</sub>-O-M<sup>+</sup> angle in **5** is 158° (K<sup>+</sup>), 154° (Na<sup>+</sup>), and 157° (Li<sup>+</sup>). For all other monodentate complexes we found that the C<sub>α</sub>-O-M<sup>+</sup> angle generally decreases with decreasing ionic radius. Thus, it appears that the smaller Li<sup>+</sup> can position itself in a more linear fashion compared to Na<sup>+</sup>, in order to optimize the electrostatic interaction, and this affords higher stability to **5Li**. The importance of adopting a linear “+ - +” geometry is discussed in ref. [15].
- [29] M. T. Rodgers, P. B. Armentrout, *Mass Spectrom. Rev.* **2000**, *19*, 215.
- [30] T. Wyttenbach, M. Witt, M. T. Bowers, *Int. J. Mass Spectrom.* **1999**, *182*, 243.
- [31] M. E. Bier, J. C. Schwartz in *Electrospray Ionization Mass Spectrometry: Fundamentals Instrumentation and Applications* (Ed. R. B. Cole), Wiley, New York, **1997**, pp. 235–289.
- [32] Gaussian98, revision A11.3, M. J. Frisch, G. W. Trucks, H. B. Schlegel, G. E. Scuseria, M. A. Robb, J. R. Cheeseman, V. J. Zakrzewski, J. A. Jr., Montgomery, R. E. Stratmann, J. C. Burant, S. Dapprich, J. M. Millam, A. D. Daniels, K. N. Kudin, M. C. Strain, O. Farkas, J. Tomasi, V. Barone, M. Cossi, R. Cammi, B. Mennucci, C. Pomelli, C. Adoma, S. Clifford, J. Ochterski, G. A. Petersson, P. Y. Ayala, Q. Cui, K. Morokuma, D. K. Malick, A. D. Rabuck, K. Raghavachari, J. B. Foresman, J. Cioslowski, J. V. Ortiz, A. G. Baboul, B. B. Stefanov, G. Liu, A. Liashenko, P. Piskorz, I. Komaromi, R. Gomperts, R. L. Martin, D. J. Fox, T. Keith, M. A. Al-Laham, C. Y. Peng, A. Nanayakkara, C. Gonzalez, M. Challacombe, P. M. W. Gill, B. Johnson, W. Chen, M. W. Wong, J. L. Andres, C. Gonzalez, M. Head-Gordon, E. S. Replogle, J. A. Pople, Gaussian, Inc., Pittsburgh, PA, **2002**.
- [33] A. P. Scott, L. Radom, *J. Phys. Chem.* **1996**, *100*, 16502.
- [34] E. D. Glendening, A. E. Reed, J. E. Carpenter, F. Weinhold, NBO version 3.1.
- [35] J. K. C. Lau, C. H. S. Wong, P. S. Ng, F. M. Siu, N. L. Ma, C. W. Tsang, *Chem. Eur. J.* **2003**, *9*, 3383.

Received: August 10, 2004

Revised: March 29, 2005

Published online: July 1, 2005